ADVANCED WAVEFORM SIMULATION FOR SEISMIC MONITORING EVENTS

Donald V. Helmberger[1], Jeroen Tromp[1], and Arthur J. Rodgers[2]

California Institute of Technology[1] and Lawrence Livermore National Laboratory[2]

Sponsored by National Nuclear Security Administration
Office of Nonproliferation Research and Engineering
Office of Defense Nuclear Nonproliferation

Contract No. DE-FC52-06NA27319[1,2]

ABSTRACT

To lower monitoring thresholds to detect and locate small seismic events and identify nuclear explosions from natural seismicity maximum information must be extracted from limited available data. For small events (M<4.0) only a few stations may observe the event above background noise at regional or far-regional distances. Additional information on the location, depth and source is embedded in the waveforms, but isolating their contributions proves difficult. Three-component recording at two stations coupled with a few P-wave picks is sufficient to refine locations, depth, and source parameters. Several methodologies have been attempted to address these seismograms mainly associated with either calibration or wave equation analysis. While satisfying the wave equation has intellectual merit, the great complexity of the earth continues to limit its usefulness, especially at higher frequency. In contrast, calibration methods seem to be the most practical in solving the problems involving the location and identification of small events. Note that some of the best small event discriminants involve the excitation of energy in the 5 to 10 Hz range where waveform modeling is in its infancy. Moreover, if some calibration events are available, the coda magnitude methodology developed by Mayeda and his colleagues proves very useful. To extend this calibration method to moment-rate estimates requires additional information about source time histories of the calibration events, where a cluster of different size events (main plus aftershocks) becomes particularly useful.

Our main objective is to join these two approaches by using waveform modeling at the longer periods, station-path timing corrections, and frequency-dependent amplitude corrections at frequencies above .5 Hz. In particular, we have made some progress by using 3 to 15s periods to develop 2D phase delay corrections (Maps) for Airy Phase Rayleigh and Love Waves for Southern California. Three component recordings at two stations coupled with a few P-wave picks proves very effective to refine locations, depths, and source parameters when compared against results for 150 stations. For still smaller events, we developed a method to work in the .5 to .2 Hz band (essentially the short-period band), and invert P-waveforms for source parameters down to $M_w = 2$ using station calibration. These events can be used to calibrate P-waves for still smaller events working in the 8 to 2 Hz range. This allows the modeling of short-period array P-wave data where numerous events can be examined in terms of source excitation, mining blasts, small explosions, major accidents, etc. Accurate estimates of m_b (P-wave energy) can be used in combination with SP/LP ratio, Woods and Helmberger (1997) to produce an effective discriminant for small magnitudes.

OBJECTIVE

Our main objective is to develop methods for locating and identifying seismic events, focusing primarily on earthquakes but including mining blasts and explosions. To advance methodologies, we want to use our computational resources to address both deterministic approaches as well as developing a better physical understanding of scattering where frequency-dependent coda magnitudes prove so effective. While the latter is apparently source-radiation pattern free (above some cut-off frequency), the direct phases are not and thus the combination should be even more effective in discrimination. In this report, we concentrate on the direct phases and produce a very well recorded set of events ($2<M<5$) which can be used for calibration and scattering models.

RESEARCH ACCOMPLISHED

We begin with a brief review of modeling and how we intend to use the larger events ($M>3.5$) as "Master events" to select simple paths and develop frequency-dependent station corrections. These refinements can then be used to address directivity effects for the larger events ($M>3.5$).

Our basic idea is to explore the large number of seismic stations in Southern California (SC) to develop useful techniques. Since earthquake occurrence in Southern California has been one of the highest in the world, we have a natural laboratory to observe seismic wave complexity generated by different types of earthquakes in a variety of tectonic settings. The number of events recorded is huge but the earthquake catalog Southern California Seismic Network (SCSN) is still dominated by information generated by the short-period array, namely, location and focal-mechanism plots based on travel time and first motion polarity picks. The relative locations has greatly increased in resolution with the cross-correlation methodology, where the first few seconds of P-waves are used in establishing onset timing differentials, Waldhauser and Ellsworth (2000) and Shearer et al. (2005). More recently, the latter researchers have used this same window to estimate Brune-type source parameters with considerable success.

The change over from short-period vertical-type seismology to broadband waveform modeling is facing considerable challenges caused by propagational complexity. At long-periods, LP>6s, these features are less severe and have been modeled remarkably well even for regions along the extended Los Angeles basin, Liu et al. (2004) and Tromp et al. (2005). However, automated methods still use longer period surface-waves and apply a CMT-type solution. These solutions for larger events agree well with the Harvard Centroid Moment Tensors but apparently agree less well with the depth estimates given in the SCSN files. The sensitivity of long-period surface-wave to depth is relatively low. A more accurate determination is possible with the use of depth phases, Helmberger and Wood (1996). Thus including bodywaves into source inversions proves quite useful in constraining possible solutions and are combined in a hybrid method developed by Zhao and Helmberger (1994). This approach called the "cut and paste" (CAP) method breaks the seismograms into segments, upper panel of Fig. 1, and fits the waveforms independently. Synthetics for a model, 1D in this exercise, are stored as a function of distance and depth for the fundamental fault systems, strike-slip, dip-slip, and 45° dip-slip. Combinations of these three synthetics based on weighting determined by possible strike (θ), slip (λ), and dip (δ) are used to obtain the best solution, Zhao and Helmberger (1994), Zhu and Helmberger (1996), and Tan and Helmberger (2006). The source mechanism is obtained by applying a direct grid search through all possible combinations to find the global minimum of misfit between the data and synthetics. In this search, a range of time shifts are allowed between portions of the seismograms when correlating with synthetics to account for crustal variation not included in the model. For example, the observed Pnl waves (extended P-waves) are too early by .7s at PAS and by .36s at GSC, see Fig. 2 for a phase delay map used to predict these delays for surface waves. The cross-correlation values are given in the second row of numbers. The best depth is obtained by fitting a curve through the best fitting grid solutions, and estimating the minimum.

The bottom of Fig. 1 displays how two stations can be used to determine location, depth, origin time, and mechanism simultaneously. The white lines show possible locations based on the P-wave travel time picks for these two stations. If station delays are small, the preferred location would fall along the slice (±.05). If there are delays at any one station, the location will be shifted as displayed. If we knew the surface waves travel time delays, we could also search for the best combination of unknowns by allowing the source to be

situated at every node in a cube and searching for the best mechanism for that position, *Tan et al.* (2006). Adding P-waves with calibrated paths greatly strengthens this approach by fixing the location and nodes. The surface waves then help to fix the depth and moment. We think such a methodology can be used to study events with the sparse datasets, especially when combined with coda-magnitudes.

The rapid expansion of TriNet array has allowed applications of the earlier developed techniques to a much larger data set, Tan and Helmberger (2006), where we have retrieved the source parameters of 250 earthquakes that occurred between 1998-2005 with the so-called "cut and paste" source estimation technique. The two-station methodology was used at the two stations, PAS and GSC (Fig. 1) and tested against the results of the full array. Nearly 80% of the events can be located by these two stations to within 5 km with accurate depth and mechanism estimates, using the phase-delay maps for Love and Rayleigh waves as in Fig. 2. This particular map was generated directly from modeling local events but given the similarity of Fig. 2 with tomographic imaging, Figure 1 of Ritzwoller et al. (2005), it appears they can be generated by synthetic means which will be discussed in the poster. Moreover, high resolution models are presently being developed for particular regions, Rodgers et al. (1999). Although retrieving source mechanisms of magnitude ~3.5 or above events has become a routine process with redundant waveform data from the dense TriNet array, smaller events can hardly be addressed by such long-period (>5 sec) inversions due to the poor signal to noise ratio. Moreover, the second order source characteristics of the magnitude 4 events, such as finite fault and rupture directivity, remain unresolved in the long-period frequency band.

An effective way to address these problems is to model waveform data at shorter periods. However, the unmodeled structural effect often becomes overwhelming, where one has to face the inherent trade-offs between source complexity and structural heterogeneity. Under such circumstances, analyzing clustered events of different sizes provides a practical way to "separate" the source from the structural effect. Figure 3 displays a typical comparison between the records at the same station GSC from three clustered events near Big Bear. While the smaller events are depleted in long-period (5-20 sec) energy, all the three events display very similar signals in the higher frequency bands. This implies propagational stability along the path. Although what has caused the complexity is unclear, the most important information conveyed in Fig. 3 is the possibility of a "two-way" calibration process. First, we can use the magnitude 4 event with the known source mechanism to calibrate the path effect on short-period records, so that smaller events can be studied. Secondly, the smaller events can provide empirical Green's functions at high frequency for studying the detailed rupture process of the big event. Although we only address events with magnitude down to two here, the same methodology has a potential for even smaller events working in the 2 to 8 Hz window.

a) Determining mall earthquake focal mechanisms using high frequency P-waves

In this section, we will demonstrate the two major steps in terms of using high frequency P-waves, namely, path calibration, and short period P-wave inversion. We concentrate on the first P arrival (mainly P_g and P_n phases), since they are the most easily isolated and understood in terms of crustal complexity. The frequency band of 0.5-2Hz is selected, where small events with M_L down to ~2.0 have good signal to noise ratio, while detailed rupture processes of bigger events are mostly filtered out.

The 2003 Big Bear sequence started with a magnitude 5 mainshock and produced about 100 aftershocks with magnitudes down to 2 in the following couple of months. Among them, six events have adequate signal to noise ratio for the LP inversion. The discrepancies between the observed P-waves and the synthetics in the SP-band are mainly manifested as amplitude differences. For quantification purposes, we define the function of "Amplitude Amplification Factor" (AAF) as

$$AAF = \sqrt{\frac{\int u^2(t)\,dt}{\int s^2(t)\,dt}}, \qquad (1)$$

where u(t) and s(t) are the data and synthetics, respectively. The integration is over a 2 sec window centered on the onset of P wave. It appears that the most anomalous AAFs occur for the stations in the basins. In particular, these stations are consistently characterized by large AAFS (>1) on the vertical component, but small AAFs (<1) on the radial component. This discrepancy between the vertical and radial components has been noted by many previous investigators (e.g., Savage and Helmberger, 2004). By comparing the AAFs derived from all the calibration events, particularly, the thrust and the strike-slip events, we found a large number (~70) of stations display stable, and mechanism-independent AAFs, which suggest the amplitude discrepancy of the synthetic P-waves could be corrected to model the observations, hence determine the earthquake focal mechanism.

We invert the short-period P waves with a similar grid-search approach as in the long-period inversion, where we minimize the L2 norm of the misfit between the data and synthetics:

$$e = \left\| u(t) - AAF \,.\, s\,(t) \right\|. \tag{2}$$

The AAFs in equation (1) are taken as the averages of the AAFs derived from the calibration events. The validation test with respect to the calibration events shows remarkable agreement between the results from short-period P-wave inversions and their known LP solutions (Tan and Helmberger, 2006a). Moreover, the advantage of adding the AAF corrections is clearly displayed in Fig. 4 where the results with and without the AAF corrections for the calibration event 13936432 are compared. Note that this works for events independent of mechanism indicating that the correction is primarily caused at the station. We also conducted statistic tests on the calibration events using subsets of the recording stations to mimic the poor coverage smaller events will face, in an attempt to quantify how many stations are needed for a reliable solution. We have demonstrated that one would need 15 stations, or 10 stations with the largest azimuthal gap less than 90° to obtain accurate results, (Tan and Helmberger, 2006). Although we have used only regional data, any distance can be included to enhance coverage, including far-regional and teleseismic, if calibrated in the SP-band.

With reasonably accurate mechanisms of small events, we can greatly increase the population and generate record sections of events at a single station, (see Figure 5). These events ranges in magnitude from 2.1 (13936196) to 5.1 (13935988). The top two-thirds are mostly small strike-slip events with similar seismograms. The lower portion of the section contains some larger events with some thrust events (bottommost trace), with changes in polarities in secondary arrivals.

b) Rupture Directivity

A direct consequence of rupture propagation on a fault plane is the azimuthal dependence of the observed source time function (STF). In brief, if a seismic station is located along the rupture propagation direction, the STF is narrower and has higher amplitude. For a station located such that the rupture is propagating away from it, the STF will be spread out and have a smaller amplitude. Instead of using inaccurate Green's functions, Hartzell (1978) demonstrated the feasibility of modeling the strong ground motion of a large earthquake using records from its own aftershocks as Green's functions. This empirical Green's function (EGF) approach assumes the large event and the EGF events occur at a similar location and have a similar focal mechanism, so that they share nearly the same propagational effect, and a linear scaling between their source terms exists at the same stations. Since we can rotate an aftershock to be the same mechanism as the target event, the method becomes particularly useful. We estimate the relative source time function, RSTF (t), specified by the convolution of two triangles, rise time and rupture time. We force the rise time to be independent of azimuth and solve by grid search. We illustrate the process in Fig. 6 for event 13937492, third trace from the bottom of Fig. 5, for a sample of azimuths. Preliminary results from Tan and Helmberger (2006b) indicate that most events larger than 3.5 have recognizable patterns but events in clusters show a great deal of variability in rise time (stress-drop). Because those frequencies are in the bandpass used in discriminants, they become a crucial issue for explaining anomalous data points in both energy ratio discriminants, i.e., Woods and Helmberger (1997), and P-S high frequency ratios, Walter et al. (2002).

CONCLUSIONS AND RECOMMENDATIONS

In summary, we demonstrate that regional seismograms from as few as two stations suffice to determine both the source location and mechanism provided that we have path calibration. For the 200 events tested here, the two station solutions agree well with those from the entire TriNet array except for a few cases. We also demonstrated that the magnitude 4 events with known source mechanisms can be used to calibrate the path effects on the short-period (0.5-2 sec) P waves, so that the corrected P waves can be modeled for determining focal mechanisms of the smaller events within clusters. The correction is formulated in terms of a station-specific "Amplitude Amplification Factor" (AAF), whose origin is mainly due to the site effect. Second, we show that the smaller events with radiation pattern corrections provide excellent empirical Green's functions (EGFs) for investigating the detailed rupture processes of the magnitude 4 events.

Future plans include (1) the extension of SP calibration to S-waves to constrain radiation pattern, (2) defining the portion of the recordings that are radiation pattern free (coda), (3) developing a better understanding of scattering in terms of surface structure, (4) using these measures to study mining blasts and local explosions, and (5) include the above information into a new SP/LP discriminate, Woods and Helmberger (1997) and testing at various test sites.

REFERENCES

Hartzell, S. H. (1978). Earthquake aftershocks as Green's functions, *Geophys. Res. Lett.* 5: 1–4.

Helmberger, D. V. and B. Woods (1996). Regional Source Parameters, Seismic Energy, and Discrimination, *Monitoring a Comprehensive Test Ban Treaty, E. S. Husebye and A. M. Dainty (eds.)*, Kluwer Academic Publishers: 365–383.

Helmberger, D. V., X. J. Song, and L. Zhu (2001). Crustal complexity from regional waveform tomography: Aftershocks of the 1992 Landers earthquake, California, *J. Geophys. Res.* 106: (B1): 609–620.

Helmberger, Don V. and S. Ni (2005). Approximate 3D Body-Wave Synthetics for Tomographic Models, *Bull. Seismol. Soc. Am.* 95: (1): 212–224.

Liu, Q., J. Polet, D. Komatitsch, and J. Tromp (2004). Spectral-element moment tensor inversions for earthquakes in Southern California, *Bull. Seismol. Soc. Am.* 94: 1748–1761.

Ritzwoller, Michael, N. Shapiro, M. Pasyanos, G. Bensen, and Y. Yang (2005). Short Period Surface Wave Dispersion Measurements from Ambient Seismic Noise in North Africa, the Middle East, and Central Asia, in *27th Seismic Research Review: Ground-based Nuclear Explosion Monitoring Technologies*, LA-UR-05-6407, Vol. 1, 161–170.

Rodgers, A., W. Walter, R. Mellors, A. M. S. Al-Amri, and Y.-S. Zhang (1999). Lithospheric structure of the Arabian Shield and Platform from complete regional waveform modeling and surface wave group velocities, *Geophys. J. Int.* 138: 871–878.

Savage, B. and D. V. Helmberger (2004). Site response from incident *Pnl* waves, *Bull. Seismol. Soc. Am.*, 94 (1): 357–362.

Shearer, Peter, E. Hauksson, and G. Lin (2005). Southern California hypocenter relocation with waveform cross-correlation, Part 2: Results using source-specific station terms and cluster analysis, *Bull. Seismol. Soc. Am*. 95 (3): 904–915.

Tan, Ying, L. Zhu, D. V. Helmberger, and C. Saikia (2006). Locating and Modeling Regional Earthquakes with Two Stations, *J. Geophys. Res*. 111(B1): 306–320.

Tan, Ying and D. V. Helmberger (2006a). A new method for determining small earthquake focal mechanisms using short-period P waves, submitted to *Bull. Seismol. Soc. Am.*

Tan, Ying and D. V. Helmberger (2006b). Rupture Directivity of the 2003 Big Bear aftershocks, submitted to *Bull. Seismol. Soc. Am.*

Tromp, Jeroen, Carl Tape, and Qinya Liu (2005). Seismic tomography, adjoint methods, time reversal, and banana-donut kernels, Geophys. J. Int. 160: 195–216.

Waldhauser, F. and W. Ellsworth (2000). A Double-Difference Earthquake Location Algorithm: Method and Application to the Northern Hayward Fault, California, *Bull. Seismol. Soc. Am*., 90 (6): 1353–1368.

Walter, W. R., A. J. Rodgers, M. E. Pasyanos, K. M. Mayeda, and A. Sicherman (2002). Identification in western Eurasian: Regional Body-Wave Corrections and Surface-Wave Tomography Models to improve discrimination, in *Proceedings of the 24th Seismic Research Review – Nuclear Explosion Monitoring: Innovation and Integration*, LA-UR-02-5048, Vol. 1, pp. 592–600.

Woods, B. B. and D. V. Helmberger (1997). Regional Seismic Discriminants using Wavetrain Energy Ratios, *BSSA* 87 (3): 589-605.

Zhao, L. S. and D. V. Helmberger (1993). Source retrieval from broadband regional seismograms: Hindu Kush region, *Phys. Earth Planet. Inter*. 78: 69-95.

Zhao, L.-S. and D. V. Helmberger (1994). Source Estimation from Broadband Regional Seismograms, *Bull. Seismol. Soc. Am*. 84: 91-104.

Zhu, Lupei and D. V. Helmberger (1996). Advancement in Source Estimation Techniques Using Broadband Regional Seismograms, *Bull. Seismol. Soc. Am.* 86 (5): 1634–1641.

Zhu, Lupei, D. V. Helmberger, C. K. Saikia, and B. B. Woods (1997). Regional waveform calibration in the Pamir-Hindu Kush region, *J. Geophys. Res.* 102 (B10): 22,799–22,813.

Zhu, L., Y. Tan, D. V. Helmberger, and C. Saikia (2005). Locating and Modeling Regional Earthquakes, Part I: Calibration of the Tibetan Plateau, *Pure Applied Geophys.*, in press.

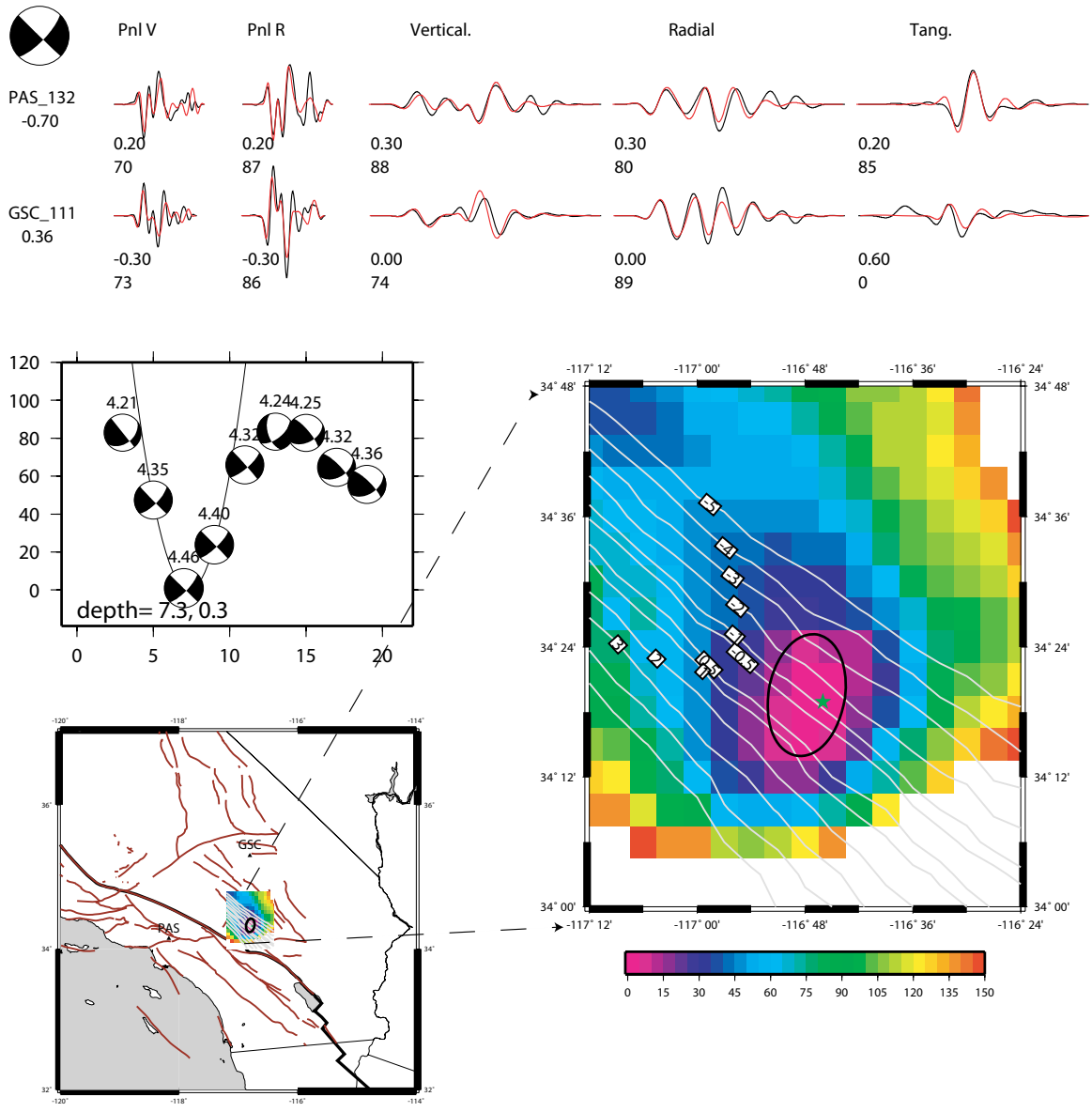

Figure 1. Demonstration of how to determine the location and mechanism simultaneously by searching various positions in a cube. The resolution based on misfit error for a 2D section at the preferred depth (7.3 km) is displayed. The various trade-offs can be seen in a 3D image. Note that if these two P-wave paths have zero corrections, we could fix the location to within a few km.

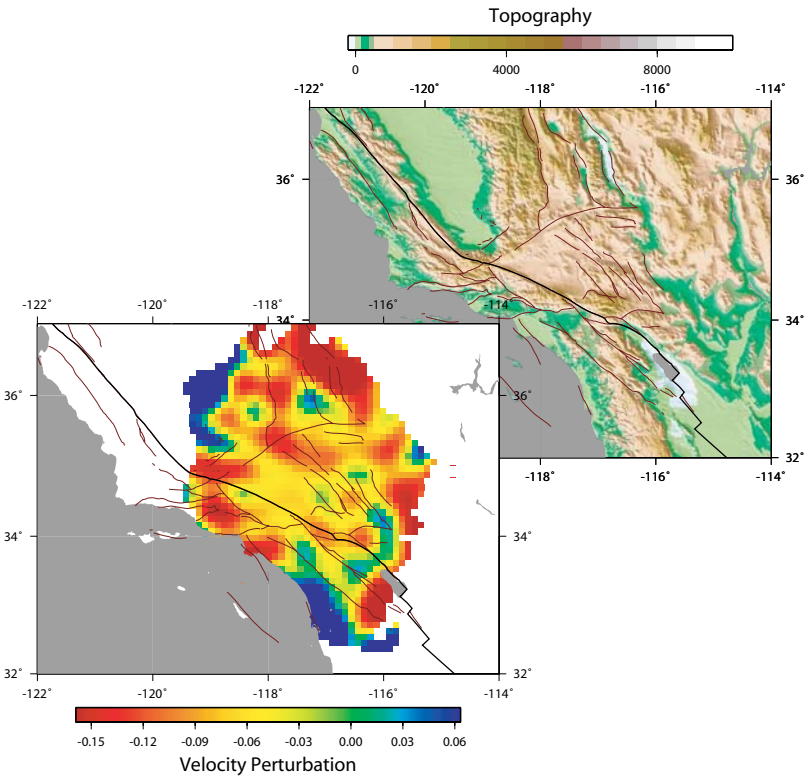

Figure 2. Comparison of the Rayleigh delay map against the topography.

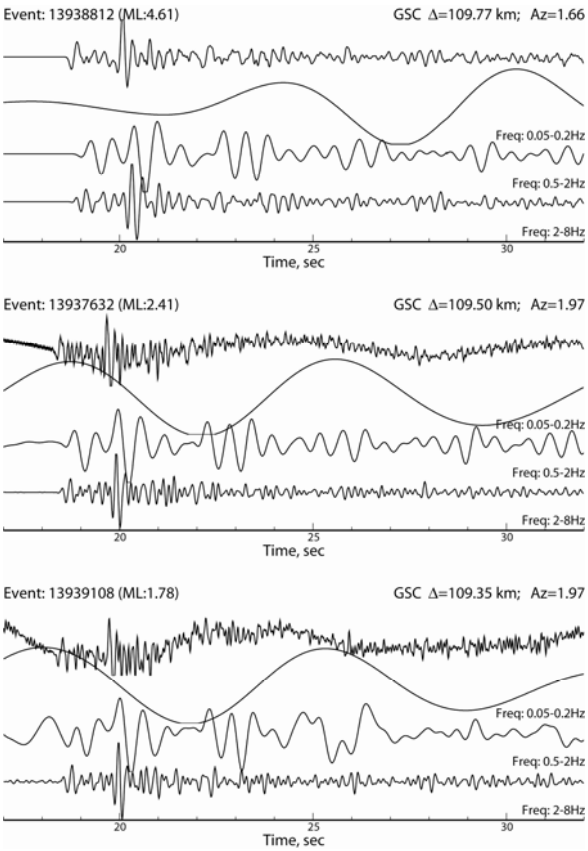

Figure 3. This figure displays the comparisons among the records from clustered, but different-sized events, M_L = 4.6, 2.4 and 1.8. For each event, the four traces from the top to bottom are the original vertical component broadband record, and the filtered records featuring different frequency bands.

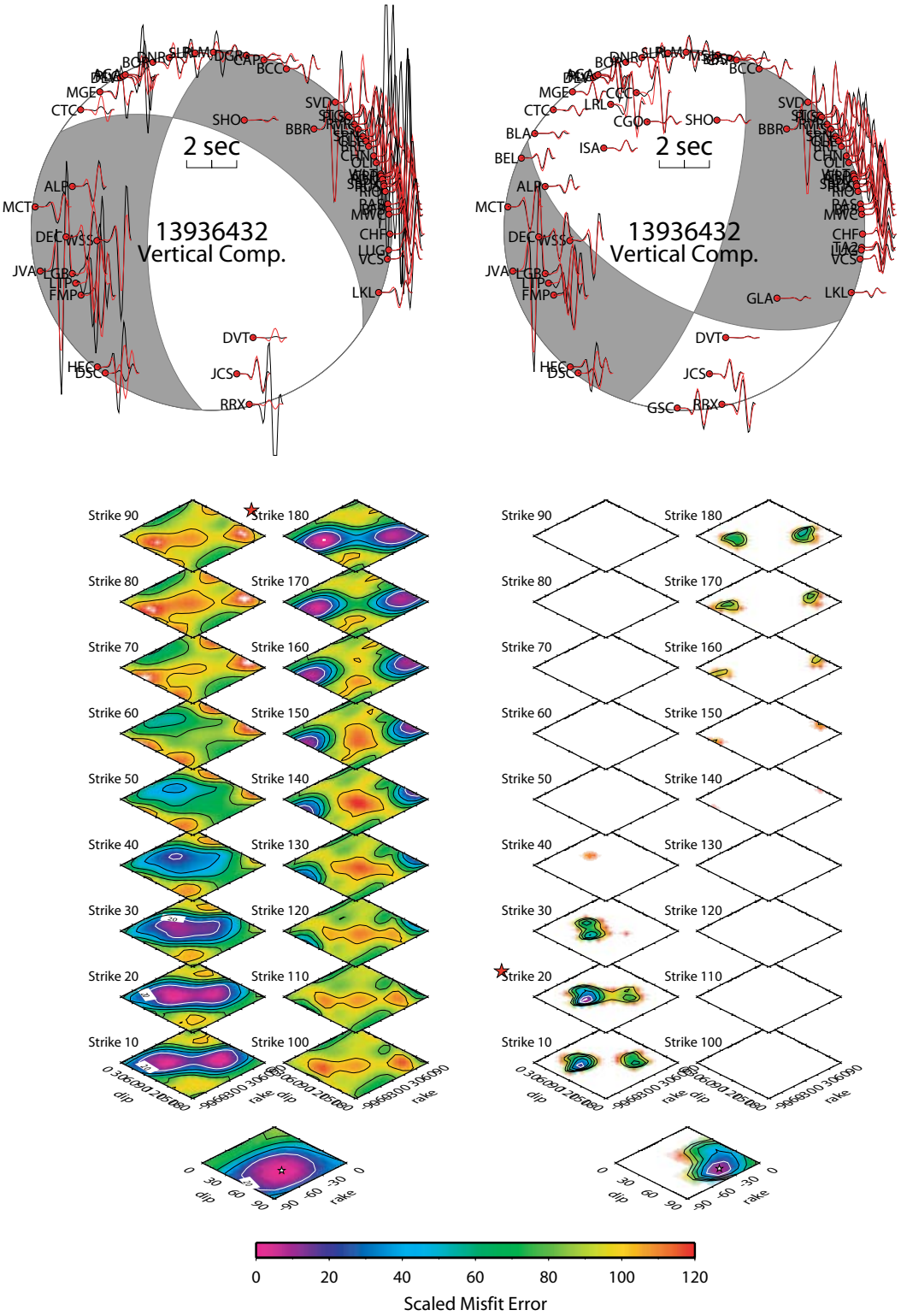

Figure 4. (Top) The resulted P-wave waveform fits on the vertical component from the short-period inversions without (left) and with AAF corrections (right) for the event 13936432 (bottom). The resolution of the solutions from short-period inversions for the event 13936432 without (left) and with AAF corrections (right) is displayed as the scaled waveform misfit errors. A red star indicates where the best solution resides with the blow up of the slice at the bottom. The white contours of 20% variance increase are displayed as the uncertainty estimates.

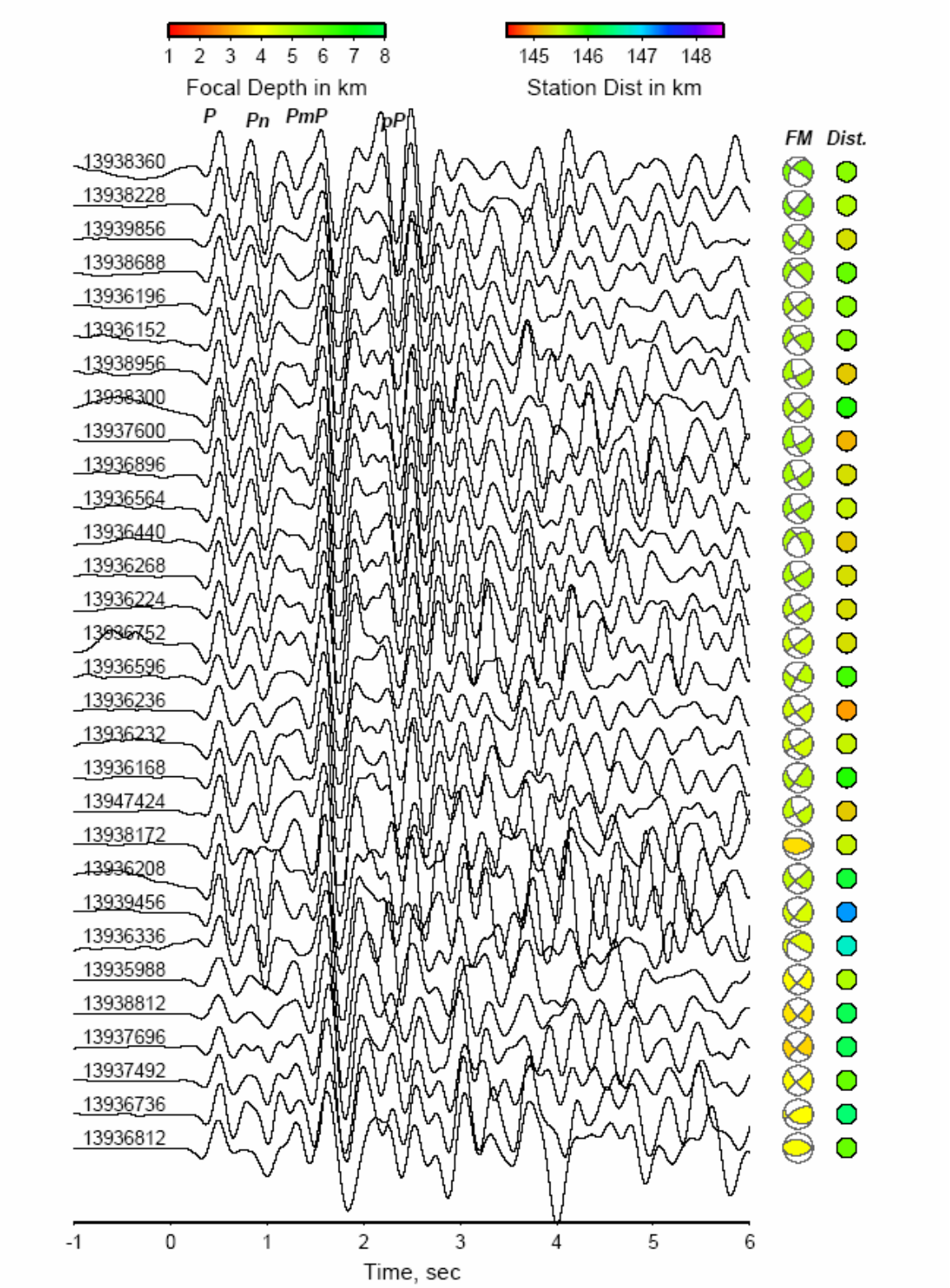

Figure 5. The vertical component records at station DPP from the clustered events of the 2003 Big Bear sequence. The traces are ordered with the separations between P and PmP increasing from the top to the bottom. Note the Pn phase changes sign for the thrust events due to the radiation pattern (bottom trace).

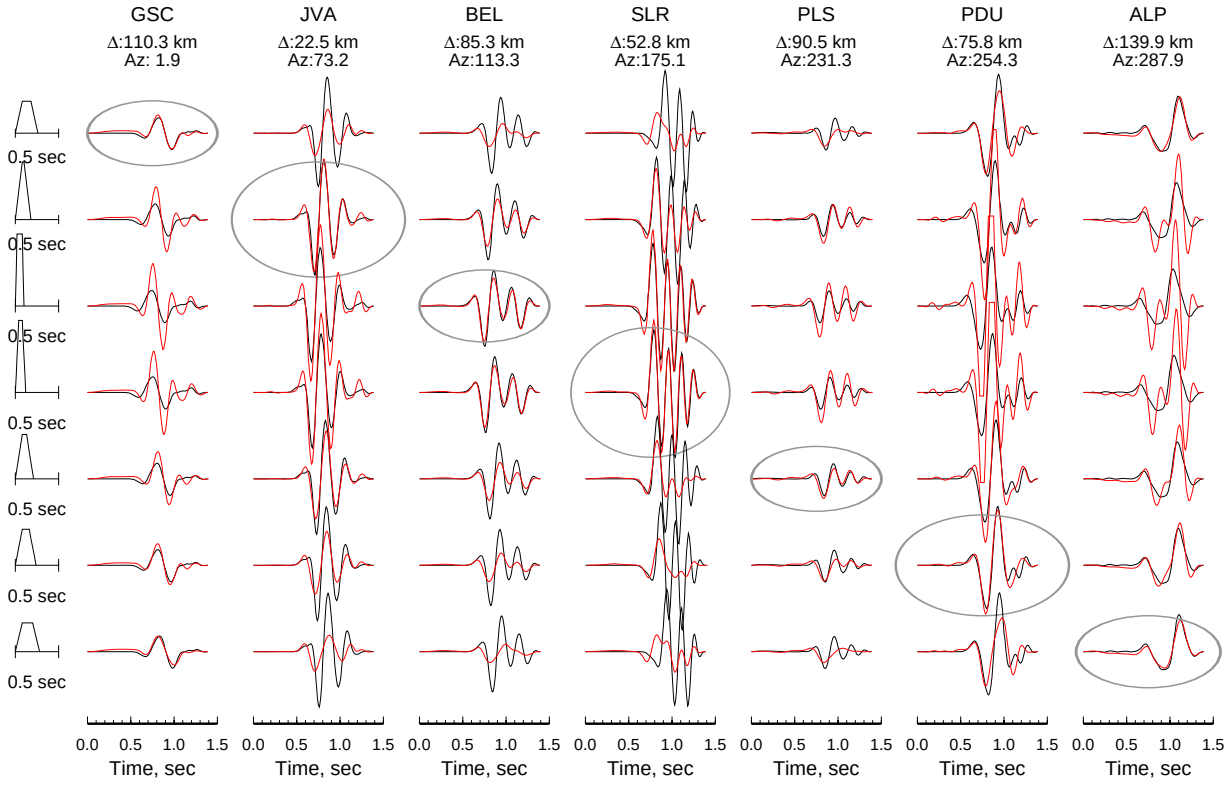

Figure 6. The selected waveform fits (Vertical P-waves) between the records from event 13937492 (black) and the "synthetics" (red) using the records from event 13937632 as EGFs. The relative source time functions (RSTFs) are given to the left. Plotted are the absolute amplitudes, except that a scaling factor of ¼, ½, and 2 has been applied to the stations JVA, PDU, and PLS respectively for the display purpose. The obtained best RSTFs for the stations are circled. Note the apparent azimuthal pattern of the RSTFs.